

Electronic Supplementary Information

Heterometallic lead-iodocuprate hybrids with transition-metal complexes:
syntheses, structures, photoelectricity and photocatalysis

Taohong Ren, Hongjin Zhu, Xiao Yang and Dingxian Jia*

College of Chemistry, Chemical Engineering and Materials Science, Soochow University, Suzhou 215123, China.

1. General methods

Elemental analysis (EA) of C, H and N was performed using an EA1110-CHNS-O elemental analyzer. Fourier transform infrared (FT-IR) spectra were recorded using a Nicolet Magna IR 550 spectrometer in the range of 4000-400 cm⁻¹ using dry KBr disks. Spectral resolution was 4 cm⁻¹, and 32 scans were averaged for each sample spectrum. Powder X-ray diffraction (PXRD) data were collected on a D/MAX-3C diffractometer using graphite monochromatic Cu-K α radiation ($\lambda = 1.5406 \text{ \AA}$) with following measurement conditions: tube voltage of 40 kV, tube current of 40 mA, stepscan mode with a 2 θ step size of 0.0334° and counting time of 0.1 s/step. Energy dispersive spectroscopy (EDS) of X-ray was performed on was recorded on a Hitachi S-4700 scanning electron microscopy. X-ray photoelectron spectroscopy (XPS) measurements were recorded on an ESCALAB 250XI spectrometer equipped with a monochromatic Al K α X-ray source (1486.6 eV). Avantage package was used for data acquisition and analysis. Calibrate all the spectra relative to a C 1s peak positioned at 284.8 eV to correct for charging effects. Then, perform deconvolution after background subtraction. Determine the elemental composition of the surfaces by calculating the atomic concentrations of each element. Then, perform deconvolution after background subtraction. Optical diffuse reflectance spectra of powder samples at room temperature were determined by a Shimadzu UV-3150 spectrometer scanning photometer. The absorption (a/S) data are calculated by reflectivity, using the Kubelka-Munk function $F(R) = (1-R)^2/2R$, where R is the reflectance at a given energy.¹

2. Photocurrent response and cyclic voltammogram measurements.

Both the photocurrent response and cyclic voltammetry measurements were performed on a CHI760E electrochemical workstation with a standard three-electrode system. For the photocurrent response test, the sample coated ITO glass was used as the working electrode, the Pt wire as the auxiliary electrode, and the saturated calomel electrode (SCE) as the reference electrode. The working electrode was prepared as following steps: 10 mg of the as-prepared sample and 10 μ L Nafion solution (5 wt%) was dispersed in 1 mL absolute ethanol and ultrasonically stirring for 1 h to form a homogeneous colloid. The colloid is coated between two ITO glasses with an effective area about 1 cm^2 , and then, the ends of two ITO glasses were sealed by conductive adhesive. The Na_2SO_4 aqueous solution ($0.05 \text{ mol}\cdot\text{L}^{-1}$) was used for supporting electrolyte solution. The light source was a 200 W high-pressure xenon lamp, which is placed about 10 cm from the surface of the ITO electrode. Cyclic voltammetry was performed in a DMF solution of tetrabutylammonium hexafluorophosphate ($0.1 \text{ mol}\cdot\text{L}^{-1}$) with a scan rate of $100 \text{ mV}\cdot\text{s}^{-1}$.

3. Photocatalytic Experiments.

The photocatalytic activities of the samples **1-3** were studied by the degradation of organic dyes in aqueous solution under visible light irradiation of a 200 W Xe lamp with a cutoff filter of below 400 nm. The as-prepared sample (25 mg) was added to 150 mL of organic dye solution ($1\times 10^{-5} \text{ mol}\cdot\text{L}^{-1}$), and then the solution was magnetically stirred in the dark for 30 min to establish adsorption/desorption equilibrium. The vertical distance between the dye solution interface and the xenon lamp source was kept at 10 cm. During the photodegradation, about 7 mL of suspension was taken away from the reaction at certain time interval and separated by centrifugation for UV-vis absorption spectroscopy measurements. The UV-vis absorption spectra of the dye solutions were measured on a PE Lambda 35 UV/vis spectrophotometer.

4. Electron paramagnetic resonance measurements.

Measurement of electron paramagnetic resonance (EPR) was conducted on an electron spin resonance spectrometer JES-X320 (Japan). The signals of DMPO-•O²⁻ and DMPO-•OH (DMPO = 5,5-dimethyl-1-pyrroline N-oxide) free radicals were captured in CH₃OH and H₂O system. The mixed solution of 400 μ L DMPO (56 μ L, 98%) and CH₃OH or H₂O (10 mL) was measured, and 2 mg catalyst was added. Homogeneous reaction was initiated by ultrasound for 5 min. The signal of

TEMPO-h⁺ (TEMPO = 2,2,6,6-tetramethylpiperidine-1-oxy) free radical signal was captured in H₂O system. The mixed solution of 400 μL TEMPO (56 μL, 10 mM) and H₂O (10 mL) was measured, and 2 mg catalyst was added. Homogeneous reaction was initiated by ultrasound for 5 min. The above two homogeneous solutions were transferred to a quartz capillary (0.5 mm), sealed at the bottom of the capillary, and placed in a matching quartz detection tube for dark or light EPR test. To minimize measurement errors the same quartz capillary tube was used throughout the EPR measurements.

Table S1 Crystallographic data and refinement parameters of compounds **1-3**

	1	2	3
Empirical formula	C ₆ H ₂₄ N ₆ MnPbCuI ₅	C ₆ H ₂₄ N ₆ FePbCuI ₅	C ₆ H ₂₄ N ₆ NiPbCuI ₅
Formula weight	1140.48	1141.39	1144.25
Crystal system	orthorhombic	orthorhombic	orthorhombic
Space group	<i>Pna</i> 2 ₁	<i>Pna</i> 2 ₁	<i>Pna</i> 2 ₁
<i>a</i> (Å)	9.2493(5)	9.2145(18)	9.1008(18)
<i>b</i> (Å)	23.7341(13)	23.643(5)	23.247(5)
<i>c</i> (Å)	10.6004(5)	10.589(2)	10.511(2)
<i>V</i> (Å) ³	2327.0(2)	2307.0(8)	2223.7(8)
<i>Z</i>	4	4	4
<i>T</i> (K)	293(2)	223(2)	293(2)
D _c (g·cm ⁻³)	3.255	3.286	3.418
<i>F</i> (000)	2012	2016	2024
μ (mm ⁻¹)	15.290	15.505	16.279
θ range (°)	3.8970 to 25.35	3.0770 to 25.35	3.0515 to 25.35
Measured reflections	8552	20911	8562
<i>R</i> _{int}	0.0439	0.0643	0.0311
Unique reflections	4050	3978	3329
No. of Parameters	183	183	183
<i>R</i> 1, [<i>I</i> >2σ(<i>I</i>)]	0.0500	0.0473	0.0285
<i>wR</i> 2, (all data)	0.0645	0.0668	0.0581
GOF on F ²	0.956	1.114	1.040

Table S2 Selected Bond Lengths (Å) and angles (°) for **1**

Pb(1)–I(1)	3.1654(15)	Pb(1)–I(2)	3.2456(14)
Pb(1)–I(2)#2	3.4029(15)	Pb(1)–I(3)	3.2296(16)
Pb(1)–I(4)	3.1579(15)	Pb(1)–I(4)#2	3.2249(15)
Cu(1)–I(1)	2.632(3)	Cu(1)–I(2)#2	2.952(4)
Cu(1)–I(3)#2	2.611(3)	Cu(1)–I(5)	2.610(3)

Mn(1)–N(1)	2.259(15)	Mn(1)–N(2)	2.265(14)
Mn(1)–N(3)	2.277(13)	Mn(1)–N(4)	2.279(13)
Mn(1)–N(5)	2.290(13)	Mn(1)–N(6)	2.258(14)
I(1)–Pb(1)–I(2)	90.80(4)	I(1)–Pb(1)–I(2)#2	80.13(4)
I(1)–Pb(1)–I(3)	172.20(3)	I(1)–Pb(1)–I(4)#2	92.93(4)
I(2)–Pb(1)–I(2)#2	89.84(4)	I(3)–Pb(1)–I(2)	83.90(4)
I(3)–Pb(1)–I(2)#2	105.50(4)	I(4)–Pb(1)–I(1)	87.73(4)
I(4)–Pb(1)–I(2)	91.01(3)	I(4)#2–Pb(1)–I(2)	174.70(4)
I(4)–Pb(1)–I(2)#2	167.83(4)	I(4)#2–Pb(1)–I(2)#2	87.10(3)
I(4)–Pb(1)–I(3)	86.66(4)	I(4)#2–Pb(1)–I(3)	92.75(4)
I(4)–Pb(1)–I(4)#2	92.89(4)	I(1)–Cu(1)–I(2)#2	98.40(10)
I(3)#2–Cu(1)–I(1)	116.99(12)	I(3)#2–Cu(1)–I(2)#2	102.01(10)
I(5)–Cu(1)–I(1)	114.01(11)	I(5)–Cu(1)–I(2)#2	113.98(11)
I(5)–Cu(1)–I(3)#2	110.34(11)	Cu(1)–I(1)–Pb(1)	92.82(8)
Cu(1)#1–I(2)–Pb(1)	83.08(6)	Cu(1)#1–I(2)–Pb(1)#1	82.77(6)
Cu(1)#1–I(3)–Pb(1)	88.96(8)	Pb(1)–I(2)–Pb(1)#1	88.27(4)
Pb(1)–I(4)–Pb(1)#1	93.02(4)	N(1)–Mn(1)–N(2)	78.0(6)
N(1)–Mn(1)–N(3)	96.4(5)	N(1)–Mn(1)–N(4)	92.5(5)
N(1)–Mn(1)–N(5)	167.1(5)	N(2)–Mn(1)–N(3)	93.7(5)
N(2)–Mn(1)–N(4)	166.0(5)	N(2)–Mn(1)–N(5)	93.4(6)
N(3)–Mn(1)–N(4)	76.9(5)	N(3)–Mn(1)–N(5)	93.8(5)
N(4)–Mn(1)–N(5)	97.6(6)	N(6)–Mn(1)–N(1)	93.8(6)
N(6)–Mn(1)–N(2)	97.5(6)	N(6)–Mn(1)–N(3)	166.2(6)
N(6)–Mn(1)–N(4)	93.4(5)	N(6)–Mn(1)–N(5)	77.6(5)

Symmetry transformations used to generate equivalent atoms: #1 x+1/2, -y+1/2, z; #2 x-1/2, -y+1/2, z.

Table S3 Selected Bond Lengths (\AA) and angles ($^\circ$) for **2**

Pb(1)–I(1)	3.2288(15)	Pb(1)–I(1)#2	3.1764(15)
Pb(1)–I(2)	3.2508(15)	Pb(1)–I(3)	3.2665(15)
Pb(1)–I(3)#1	3.3938(16)	Pb(1)–I(4)	3.2010(15)
Cu(1)–I(2)#1	2.632(3)	Cu(1)–I(3)#1	2.924(3)
Cu(1)–I(4)	2.647(3)	Cu(1)–I(5)	2.639(3)
Fe(1)–N(1)	2.166(12)	Fe(1)–N(2)	2.135(11)
Fe(1)–N(3)	2.139(12)	Fe(1)–N(4)	2.144(13)
Fe(1)–N(5)	2.109(13)	Fe(1)–N(6)	2.154(12)
I(1)#2–Pb(1)–I(1)	91.99(4)	I(1)–Pb(1)–I(2)	92.98(3)
I(1)#2–Pb(1)–I(2)	86.19(4)	I(1)–Pb(1)–I(3)	174.98(4)
I(1)–Pb(1)–I(3)#1	88.14(3)	I(1)#2–Pb(1)–I(3)	91.31(3)
I(1)#2–Pb(1)–I(3)#1	169.16(4)	I(1)#2–Pb(1)–I(4)	88.51(3)
I(2)–Pb(1)–I(3)	83.46(4)	I(2)–Pb(1)–I(3)#1	104.63(4)

I(3)–Pb(1)–I(3)#1	89.33(4)	I(4)–Pb(1)–I(1)	93.29(4)
I(4)–Pb(1)–I(2)	171.93(3)	I(4)–Pb(1)–I(3)	90.58(4)
I(4)–Pb(1)–I(3)#1	80.66(4)	I(2)#1–Cu(1)–I(3)#1	102.54(9)
I(2)#1–Cu(1)–I(4)	118.09(12)	I(2)#1–Cu(1)–I(5)	108.93(10)
I(4)–Cu(1)–I(3)#1	99.97(9)	I(5)–Cu(1)–I(3)#1	113.04(10)
I(5)–Cu(1)–I(4)	113.49(10)	Pb(1)#1–I(1)–Pb(1)	92.10(4)
Cu(1)#2–I(2)–Pb(1)	88.28(7)	Cu(1)#2–I(3)–Pb(1)#2	82.29(6)
Cu(1)#2–I(3)–Pb(1)	83.27(6)	Pb(1)–I(3)–Pb(1)#2	87.62(4)
Cu(1)–I(4)–Pb(1)	90.51(7)	N(2)–Fe(1)–N(1)	81.2(5)
N(2)–Fe(1)–N(3)	94.4(5)	N(2)–Fe(1)–N(4)	93.3(5)
N(2)–Fe(1)–N(6)	171.8(5)	N(3)–Fe(1)–N(1)	92.8(5)
N(3)–Fe(1)–N(4)	81.4(5)	N(3)–Fe(1)–N(6)	91.7(5)
N(4)–Fe(1)–N(1)	171.7(5)	N(4)–Fe(1)–N(6)	93.1(5)
N(5)–Fe(1)–N(1)	94.1(5)	N(5)–Fe(1)–N(2)	93.4(6)
N(5)–Fe(1)–N(3)	170.3(6)	N(5)–Fe(1)–N(4)	92.4(5)
N(5)–Fe(1)–N(6)	81.2(5)	N(6)–Fe(1)–N(1)	93.0(5)

Symmetry transformations used to generate equivalent atoms: #1 x–1/2, –y+1/2, z; #2 x+1/2, –y+1/2, z.

Table S4 Selected Bond Lengths (Å) and angles (°) for **3**

Pb(1)–I(1)	3.2340(11)	Pb(1)–I(1)#2	3.3557(11)
Pb(1)–I(2)	3.2096(12)	Pb(1)–I(3)	3.2003(11)
Pb(1)–I(3)#1	3.1500(11)	Pb(1)–I(4)	3.1564(12)
Cu(1)–I(1)	2.860(2)	Cu(1)–I(2)	2.607(2)
Cu(1)–I(4)#1	2.6314(19)	Cu(1)–I(5)	2.613(2)
Ni(1)–N(2)	2.123(10)	Ni(1)–N(1)	2.123(9)
Ni(1)–N(4)	2.117(10)	Ni(1)–N(3)	2.110(10)
Ni(1)–N(6)	2.134(9)	Ni(1)–N(5)	2.115(9)
I(1)–Pb(1)–I(1)#2	89.24(3)	I(2)–Pb(1)–I(1)	83.31(3)
I(2)–Pb(1)–I(1)#2	105.07(3)	I(3)–Pb(1)–I(1)	175.02(3)
I(3)–Pb(1)–I(1)#2	88.48(3)	I(3)#1–Pb(1)–I(1)	91.55(3)
I(3)#1–Pb(1)–I(1)#2	168.97(3)	I(3)–Pb(1)–I(2)	93.01(3)
I(3)#1–Pb(1)–I(2)	85.95(3)	I(3)#1–Pb(1)–I(3)	91.54(3)
I(3)#1–Pb(1)–I(4)	88.26(3)	I(4)–Pb(1)–I(1)	90.57(3)
I(4)–Pb(1)–I(1)#2	80.73(3)	I(4)–Pb(1)–I(2)	171.45(2)
I(4)–Pb(1)–I(3)	93.42(3)	I(2)–Cu(1)–I(1)	103.06(7)
I(2)–Cu(1)–I(4)#1	117.64(8)	I(2)–Cu(1)–I(5)	109.00(7)
I(4)#1–Cu(1)–I(1)	100.36(7)	I(5)–Cu(1)–I(1)	112.64(8)

I(5)–Cu(1)–I(4)#1	113.41(7)	Pb(1)–I(1)–Pb(1)#1	87.44(3)
Cu(1)–I(1)–Pb(1)	83.32(4)	Cu(1)–I(1)–Pb(1)#1	82.31(4)
Cu(1)–I(2)–Pb(1)	87.91(5)	Pb(1)#2–I(3)–Pb(1)	91.66(3)
Cu(1)#2–I(4)–Pb(1)	89.94(5)	N(1)–Ni(1)–N(6)	93.0(4)
N(2)–Ni(1)–N(1)	81.7(4)	N(2)–Ni(1)–N(6)	94.4(4)
N(3)–Ni(1)–N(1)	93.5(4)	N(3)–Ni(1)–N(2)	92.2(4)
N(3)–Ni(1)–N(4)	81.8(4)	N(3)–Ni(1)–N(5)	92.5(4)
N(3)–Ni(1)–N(6)	171.4(4)	N(4)–Ni(1)–N(1)	92.6(4)
N(4)–Ni(1)–N(2)	171.5(4)	N(4)–Ni(1)–N(6)	92.2(4)
N(5)–Ni(1)–N(1)	172.2(4)	N(5)–Ni(1)–N(2)	93.0(4)
N(5)–Ni(1)–N(4)	93.3(4)	N(5)–Ni(1)–N(6)	81.6(4)

Symmetry transformations used to generate equivalent atoms: #1 x–1/2, –y+3/2, z; #2 x+1/2, –y+3/2, z.

Table S5 Selected H···A distances(Å) and D–H···A angles (°) for **1–3**

D–H···A	d(H···A)	d(D···A)	<(DHA)
1			
N(1)–H(1)A···I(3)#3	3.251	4.042	149.29
N(1)–H(1)B···I(5)#2	3.307	4.000	136.47
N(2)–H(2)A···I(1)#2	3.036	3.874	157.66
N(2)–H(2)B···I(3)	3.140	3.674	120.62
N(3)–H(3)A···I(2)#2	3.064	3.923	162.85
N(3)–H(3)B···I(5)#2	3.058	3.907	160.05
N(4)–H(4)A···I(5)#4	3.140	3.979	158.07
N(4)–H(4)B···I(4)#5	3.082	3.915	156.63
N(5)–H(5)A···I(2)#2	2.956	3.776	153.91
N(5)–H(5)B···I(4)#5	2.964	3.839	167.87
N(6)–H(6)A···I(5)#4	3.176	4.039	163.80
N(6)–H(6)B···I(5)#1	3.143	3.930	148.67
2			
N(1)–H(1)A···I(5)#1	3.198	4.063	164.77
N(1)–H(1)B···I(5)#2	3.064	3.853	148.85
N(2)–H(2)A···I(3)#3	2.930	3.784	161.28
N(2)–H(2)B···I(1)#4	2.922	3.805	171.65
N(3)–H(3)A···I(5)#1	3.070	3.933	163.96
N(3)–H(3)B···I(1)#4	3.109	3.941	156.37
N(4)–H(4)A···I(3)#3	3.100	3.960	163.15
N(4)–H(4)B···I(5)#3	3.015	3.862	159.73
N(5)–H(5)A···I(4)#3	3.128	3.930	151.03
N(6)–H(6)A···I(2)#6	3.311	4.062	143.68
3			
N(1)–H(1)A···I(5)#1	2.972	3.816	158.94
N(1)–H(1)B···I(1)#2	3.038	3.900	163.71
N(2)–H(2)A···I(3)#3	3.038	3.876	157.75

N(2)–H(2)B···I(5)	3.019	3.884	164.30
N(3)–H(3)A···I(5)#1	3.227	3.930	137.56
N(3)–H(3)B···I(2)	3.216	3.984	145.91
N(4)–H(4)A···I(5)#4	3.301	4.006	137.91
N(4)–H(4)B···I(4)#2	3.100	3.901	150.69
N(5)–H(5)A···I(5)#4	3.021	3.811	148.98
N(5)–H(5)B···I(5)	3.152	4.019	165.33
N(6)–H(6)A···I(3)#3	2.880	3.760	170.05
N(6)–H(6)B···I(1)#2	2.885	3.734	160.11

Symmetry transformations used to generate equivalent atoms: **1**: #1 x+1/2, -y+1/2, z; #2 x-1/2, -y+1/2, z; #3 -x+1, -y, z+1/2; #4 -x+1/2, y-1/2, z+1/2; #5 x-1/2, -y+1/2, z+1; #6 x, y, z+1. **2**: #1 x, y+1, z; #2 -x+1, -y+1, z-1/2; #3 -x+2, -y+1, z-1/2; #4 -x+3/2, y+1/2, z+1/2; #5 -x+3/2, y+1/2, z-1/2; #6 x-1/2, -y+3/2, z. **3**: #1 -x, -y+1, z-1/2; #2 -x+1/2, y-1/2, z-1/2; #3 -x+1, -y+1, z+1/2; #4 -x+1, -y+1, z-1/2; #5 -x+1/2, y-1/2, z+1/2; #6 -x+3/2, y-1/2, z+1/2.

Table S6. Summary of Catalytic Activities in Photodegradation of Organic Dyes for Some Iodocuprates Hybrids

Compound	organic dyes	light source	irradiation time	band gaps of hybrids	degradation ratio	Ref.
^a [Me ₃ TPB][Cu ₅ I ₈]	^r MO	UV light	18 min	1.90 eV	98.5%	2
^b [(Pyrtca)Cu ₂ I ₂]	^s MB	UV light	40 min	1.91 eV	91%	3
	^t RhB	UV light	40 min		100%	
^c [Me ₃ (3-TPT)][Cu ₅ I ₈]	MO	UV light	50 min	1.72 eV	100%	4
	^u MV	UV light	80 min	1.72 eV	92%	
^d [Cu ₂ (μ ₃ -I)(L)] _n	MB	UV light	360 min	2.9-6.0 eV	92%	5
	RhB	UV light	360 min		46%	
^e [Cu ₄ I ₄ (bib) ₂] _n ·n(DMF)	MB	UV light	25 min	2.62 eV	96%	6
^g [L1''][Cu ₃ I ₆]	RhB	Xe lamp	70 min	2.10 eV	90%	7
^h (H ₂ DPMNI)·(Cu ₄ I ₆)·(CH ₃ CN)	RhB	Xe lamp	60 min	1.52 eV	95%	8
ⁱ {[hmt][Cu ₄ I ₅][H ₂ O] ₅ [NH ₄] ⁺ } _n	MB	UV light	40 min	1.55 eV	70%	9
[Me ₃ TPT][Cu ₅ I ₈]	MO	Xe lamp	100 min	1.05 eV	100%	10
[Et ₃ TPT][Cu ₅ I ₈]	MO	Xe lamp	110 min	1.02 eV	100%	
[Me ₃ TPT][Cu ₅ Br ₈]	MO	Xe lamp	60 min	1.30 eV	100%	
^j [Ce(cpb) ₄ (H ₂ O) ₄][Cu ₆ I ₉]	RhB	Xe lamp	80 min	1.82 eV	100%	11
^k [Co(tib) ₂]·[Cu ₄ I ₆]	MO	Xe lamp	100 min	2.29 eV	80%	12
^l [dedabco] ₄ (Cu ₄ I ₈) ₂ ·H ₂ O	^v CV	Xe lamp	180 min	2.24 eV	47.3%	13
^m [H ₂ tmdp] ₂ (Cu ₂ I ₅)(I)·H ₂ O	CV	Xe lamp	180 min	2.11 eV	46.5%	
ⁿ {[Hdbu]Cu ₂ I ₃ } _n	CV	Xe lamp	180 min	1.94 eV	98.0%	
^o [Pr(DMSO) ₈][Pb ₂ Cu ₂ I ₉]	MB	Xe lamp	160 min	2.37 eV	88.1%	14
	RhB	Xe lamp	160 min		43.8%	
^p [(pdc) ₄ (DMF) ₆ Pb ₄ Cu ₂ I ₂] _n	^w CR	UV light	20 min	2.68 eV	90%	15
^q [Co(2,2'-bipy) ₃]CuPb ₂ Br ₇	CV	UV light	60 min	2.07 eV	30%	16

^aMe₃(TPB) = N,N',N''-trimethyl-1,3,5-tris(4-pyridyl)benzene, ^bPyrta = pyrazine-2-thiocarboxamide, ^cMe₃(3-TPT)=N,N',N''-trimethyl-2,4,6-tris(3-pyridyl)-1,3,5-triazine, ^dHL = 1-tetrazole-4-imidazole-benzene, ^ebib = 1,4-bis(imidazolyl)butane, ^fDMF = N,N'-dimethylformamide, ^gL1ⁿ³⁺ = 1-ethyl-3,5-(1-ethylpyridin-3-niumcarbamoyl)-pyridinium, ^hDPMNI = N, N'-bis(4-pyridylmethyl)-1,4,5,8-naphthalene diimide, ⁱhmt = hexamethylenetetramine, ^jcpb = 1-(4-carboxybenzyl)-4,4'-bipyridinium, ^ktib = 1,3,5-tris(1-imidazolyl)benzene, ^ldeDABCO = N,N'-diethyl-1,4-diazabicyclo[2.2.2] octane, ^mtmdp = 4,4'-trimethylenedipiperidine, ⁿdbu = 1,8-diazabicyclo-[5.4.0]-undec-7-ene, ^oDMSO = dimethyl sulfoxide, ^pH₂pdc = 3,5-pyridinedicarboxylic acid, ^q2,2'-bipy = 2,2'-bipyridine, ^rMO = methyl orange, ^sMB = methylene blue, ^tRhB = rhodamine B, ^uMV = methyl violet, ^vCV= crystal violet, ^wCR = congo red.

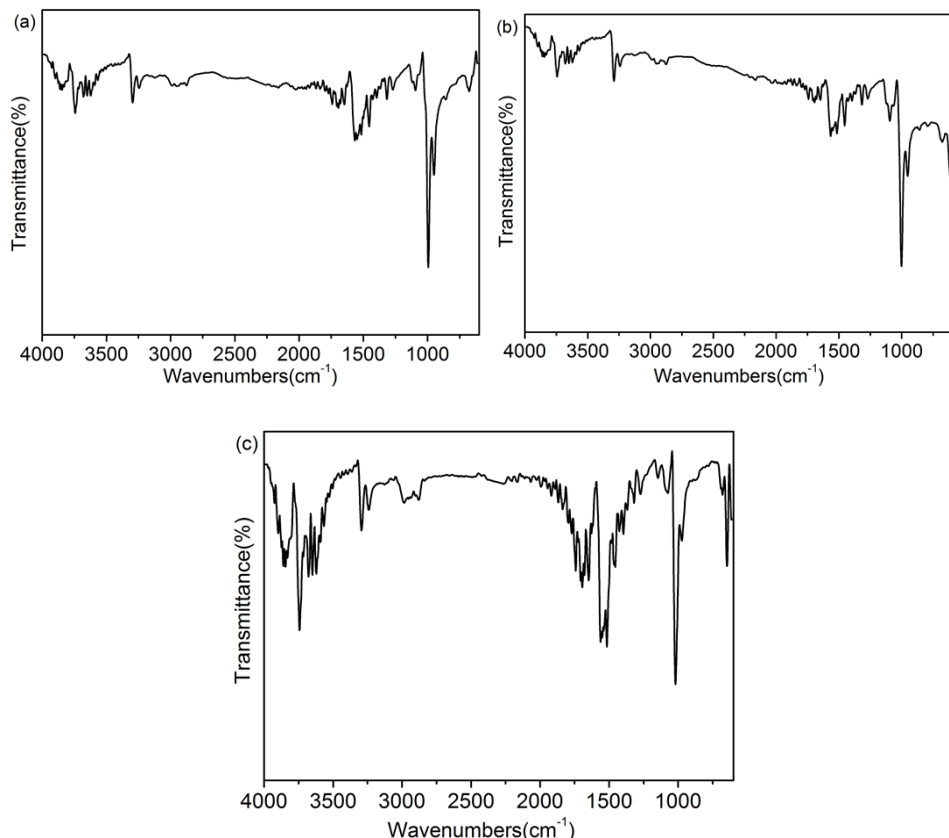


Fig. S1 IR spectra of compounds **1** (a), **2** (b), and **3** (c).

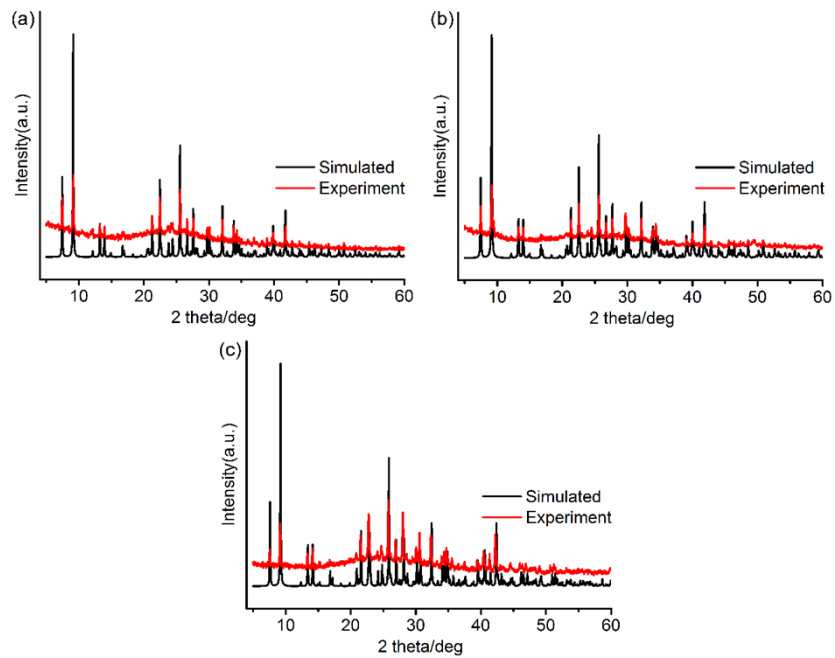


Fig. S2 Simulated and experimental powder XRD patterns of compounds **1** (a), **2** (b), and **3** (c).

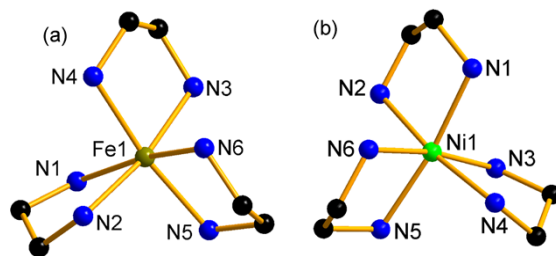


Fig. S3 Crystal structures of $[\text{Fe}(\text{en})_3]^{2+}$ (a) cation in **2**, and $[\text{Ni}(\text{en})_3]^{2+}$ cation in **3**.

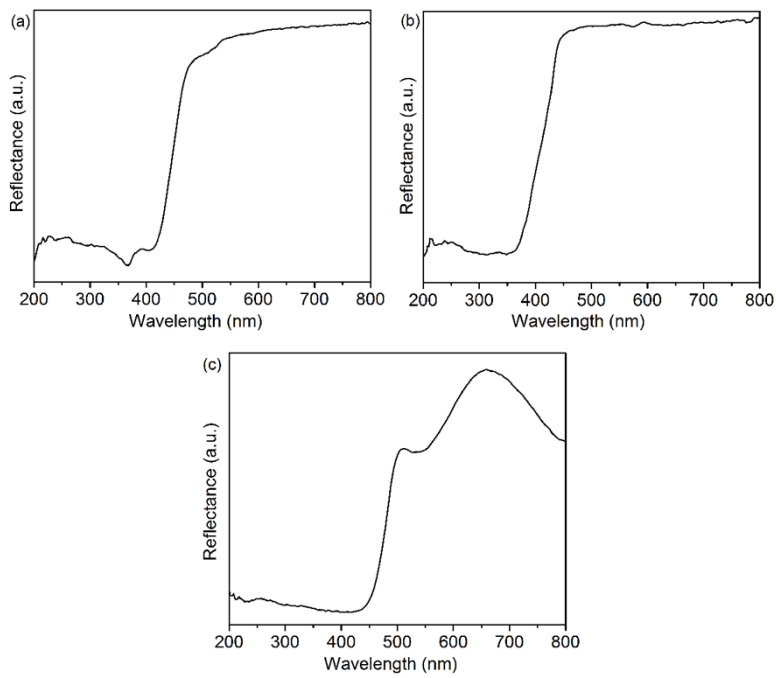


Fig. S4 Solid-state optical diffuse reflectance spectra of compounds **1** (a), **2** (b), and **3** (c).

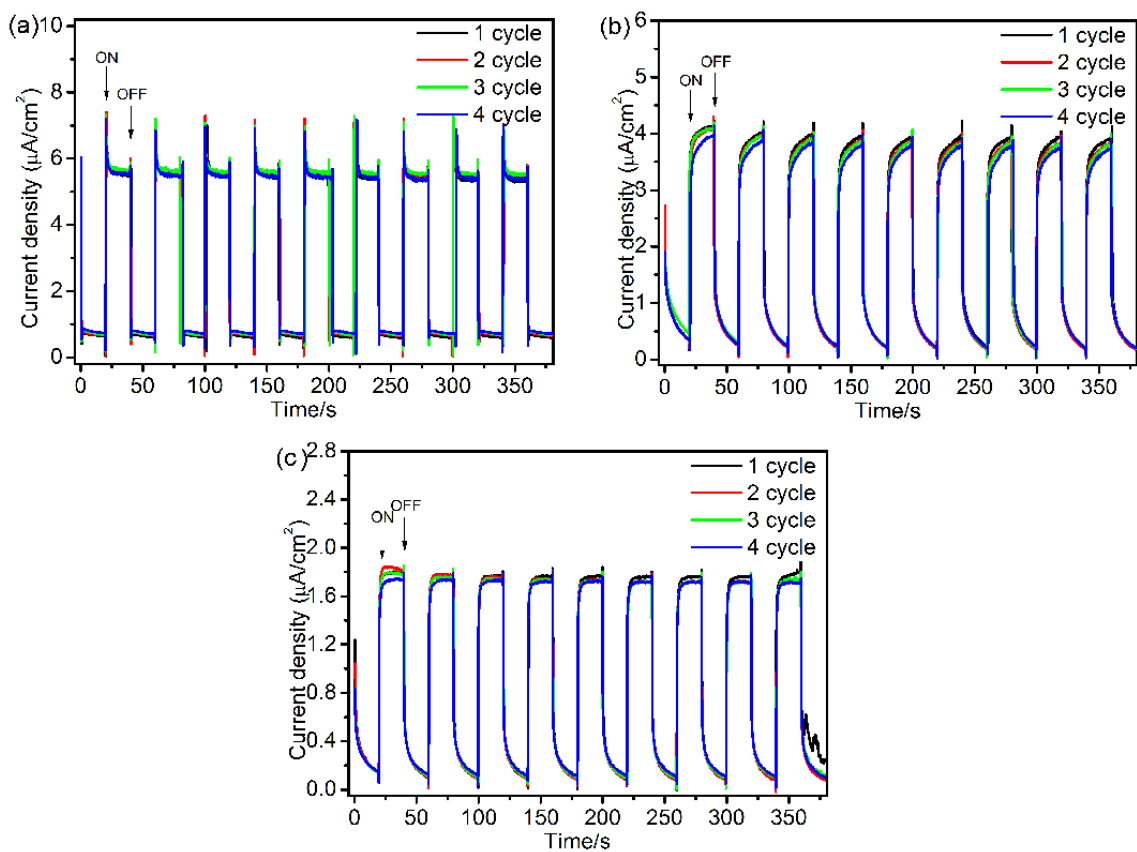


Fig. S5 Photocurrent responses of compounds **1** (a), **2** (b), and **3** (c) under illumination with light power of 200 W for four cycle measurements.

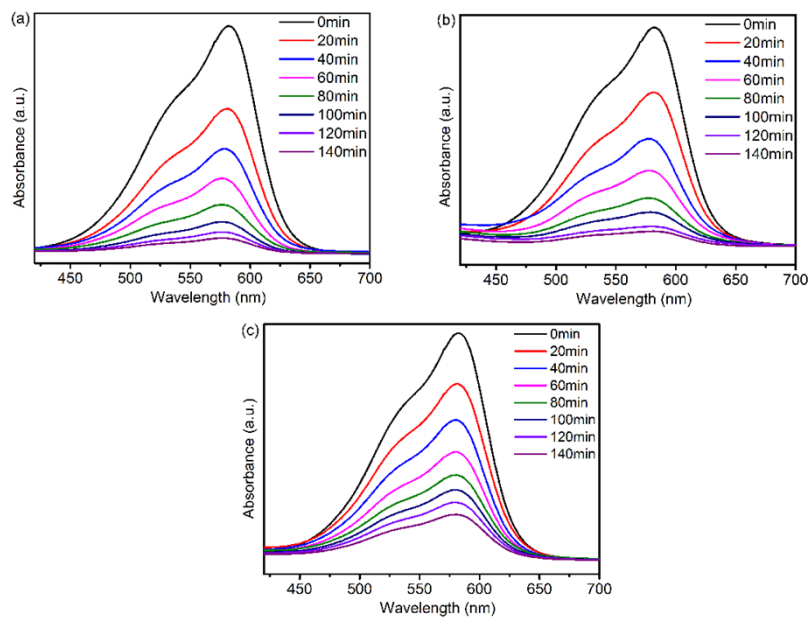


Fig. S6 Time dependent absorption spectra of CV solutions with photodegradation catalyzed by compounds **1** (a), **2** (b), and **3** (c).

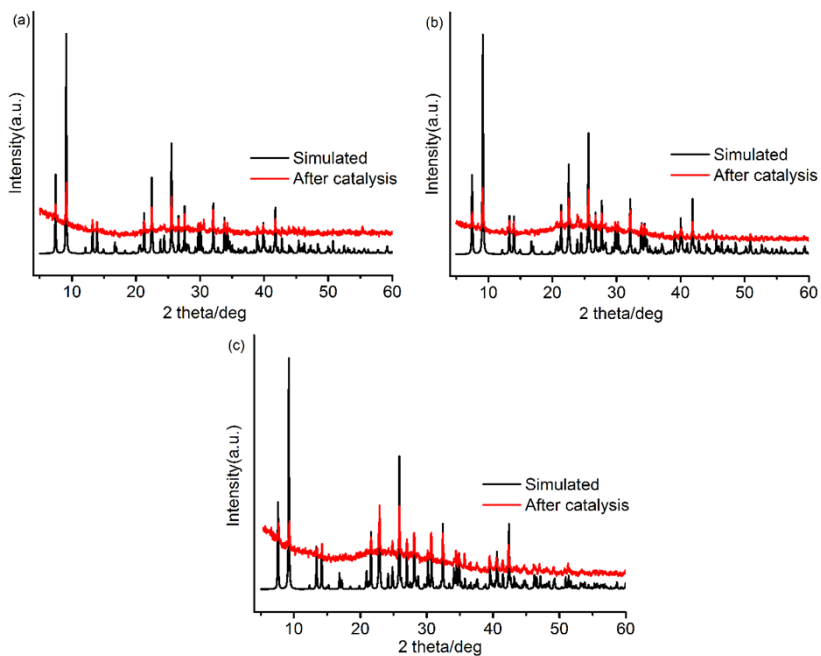


Fig. S7. Simulated PXRD patterns and experimental PXRD patterns after photocatalysis for compounds **1** (a), **2** (b), and **3** (c).

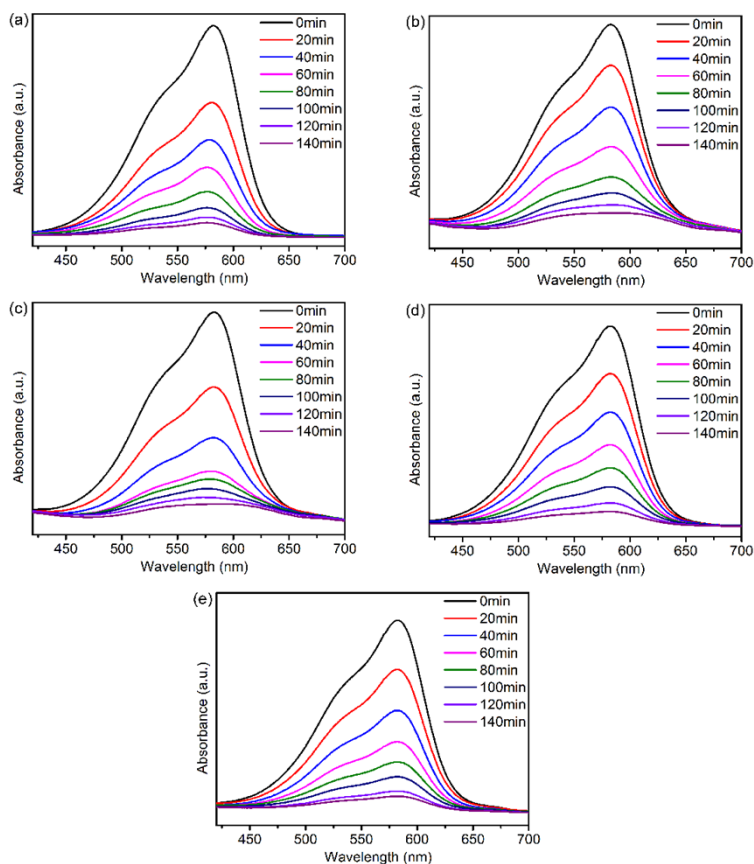


Fig. S8 Time dependent absorption spectra of CV solutions with photodegradation catalyzed by compound **1** in catalytic cycles 1 (a), 2 (b), 3 (c), 4 (d) and 5 (e).

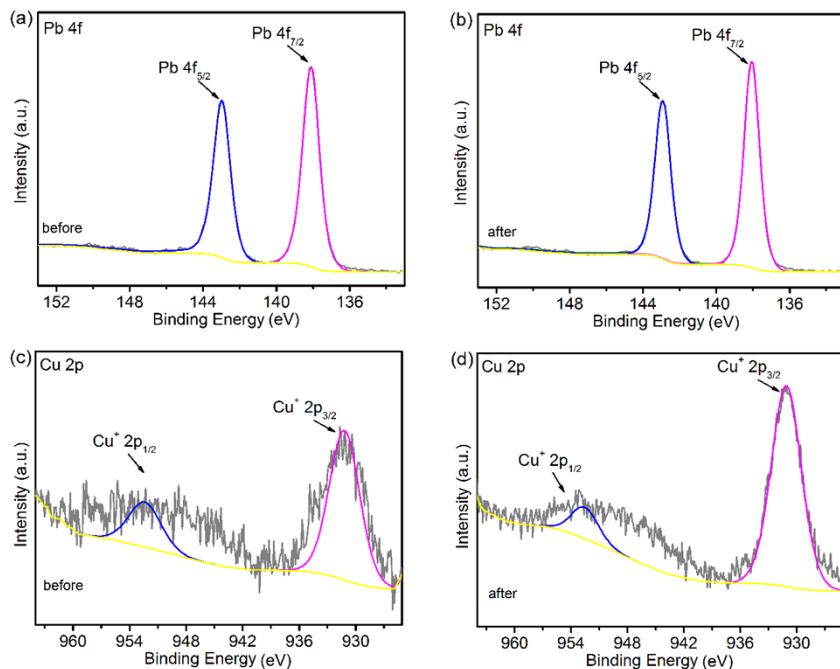


Fig. S9 XPS spectra of Pb 4f (a, b) and Cu 2p (c, d) of compound **1** before (a, c) and after (b, d)

catalysis.

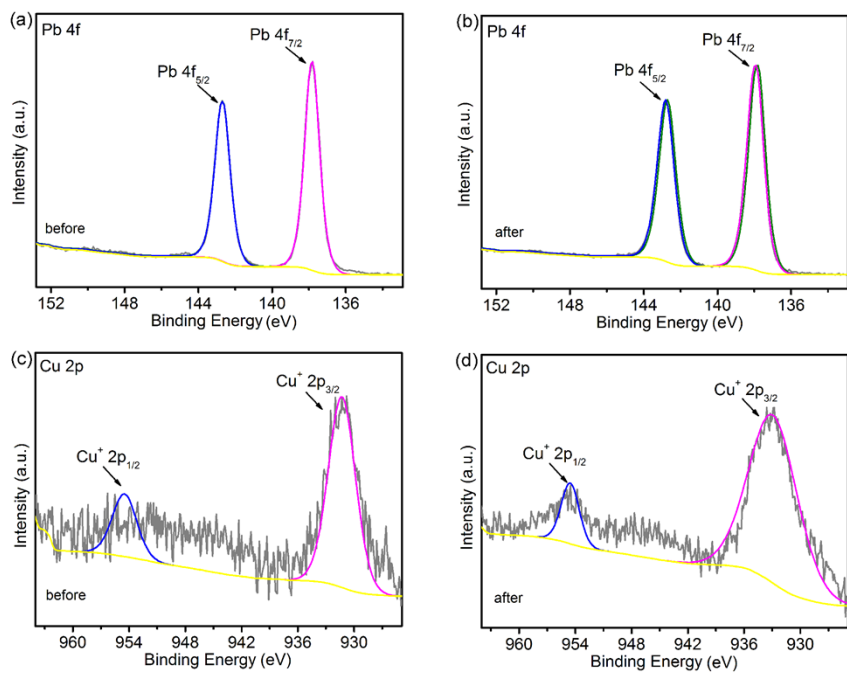


Fig. S10 XPS spectra of Pb 4f (a, b) and Cu 2p (c, d) of compound **2** before (a, c) and after (b, d) catalysis.

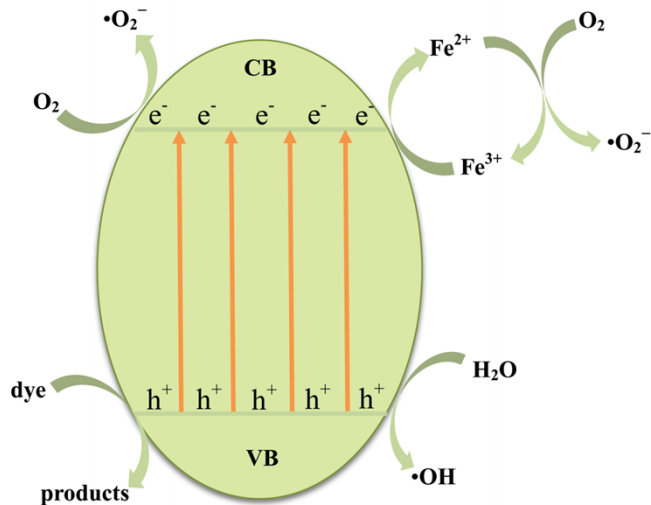


Fig. S11 Schematic diagram showing the photocatalytic mechanism for CV degradation over compound **2** under visible light irradiation.

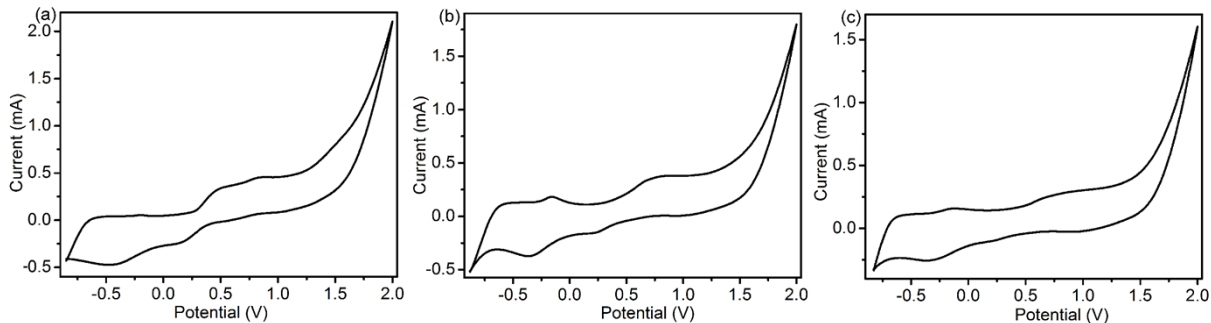


Fig. S12 Cyclic voltammograms of compounds **1** (a), and **2** (b) in DMF solution with a scan rate of $50 \text{ mV}\cdot\text{s}^{-1}$, and blank CV curve in DMF with a scan rate of $50 \text{ mV}\cdot\text{s}^{-1}$ (c).

The cyclic voltammogram behavior of compound **1** was recorded on a CHI760E electrochemical workstation using a glassy carbon electrode (GC) as working electrode. As shown in Fig. 12a, The CV curve of compound **1** shows anodic peak (E_{pa}) at 0.86 V with a current of 0.45 mA, which is attributed to the oxidation of Mn(II) to Mn(III).¹⁷ In the reverse cathodic scanning, the corresponding cathodic peak (E_{pc}) was observed at 0.18 V with a current of -0.22 mA, indicating that Mn (III) was reduced to Mn(II).¹⁸ The peak separation of ΔE_p ($E_{\text{pa}}-E_{\text{pc}}$) of 0.68 V for the Mn(III)/Mn(II) redox couple was consistent with those observed in the reported Mn(II) complexes.¹⁹ The weak anodic peak at 0.50 V in the anodic scan and the weak cathodic peak at -0.37 V in the cathodic scan of compound **1** are attributed to the anodic peak at 0.62 V and the cathodic peak at -0.32 V in the blank measurement (Fig. 12c).

The CV curve of compound **2** showed an E_{pa} at 0.74 V with a current of 0.37 mA in the anodic scanning (Fig. S12b), which was attributed to the oxidation of Fe(II) to Fe(III).²⁰ The corresponding E_{pc} at 0.24 V with a current of -0.16 mA is observed in the reversal scanning, which was anticipated to represent the reduction of Fe(III) to Fe(II) reduction.²⁰ The peak separation of ΔE_p ($E_{\text{pa}}-E_{\text{pc}}$) of 0.50 V for the Fe(III)/Fe(II) redox couple was consistent with those observed in the reported.²¹ The weak anodic peak at -0.16 V in the anodic scan and the weak cathodic peak at -0.36 V in the cathodic scan belong to the peaks in the blank experiment.

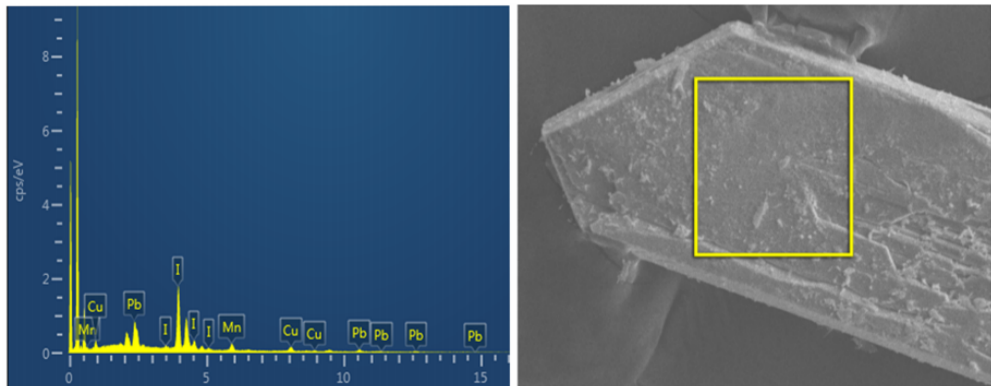


Fig. S13 EDS spectrum of compound 1.

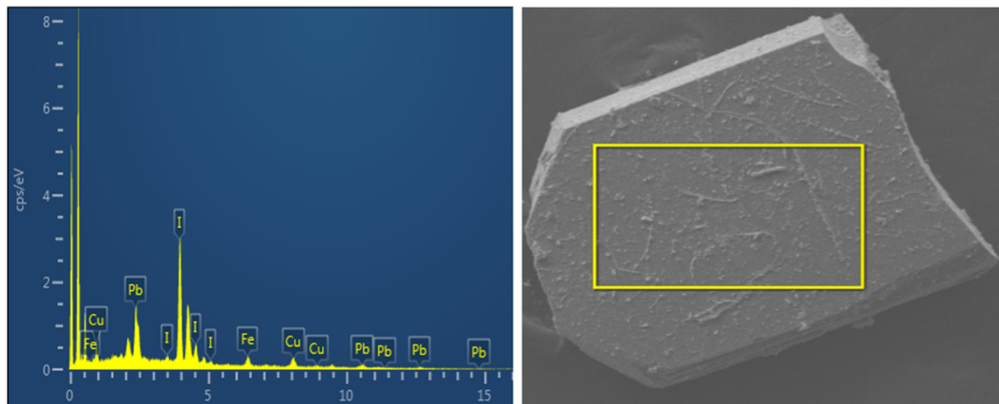


Fig. S14 EDS spectrum of compound 2.

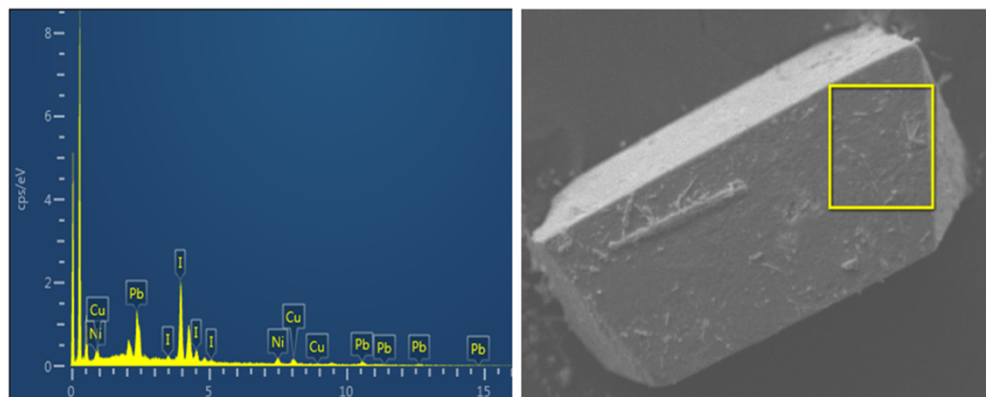


Fig. S15 EDS spectrum of compound 3.

Reference

1. W. W. Wendlandt and H. G. Hecht, *Reflectance spectroscopy*, interscience publishers, New York, **1966**.
2. X. F. Jiang, Q. Wei, B. D. Ge, A. P. Fu, J. H. Li and G. M. Wang, *Opt. Mater.*, 2020, **109**, 110376.
3. M. Murillo, A. G. Hernan, J. López, J. Perles, I. Brito and P. A. Ochoa, *Catal. Today*, 2023, **418**, 114072.
4. Q. Wei, B. D. Ge, J. Zhang, A. H. Sun, J. H. Li, S. D. Han and G. M. Wang, *Chem. Asian J.*, **2019**, **14**, 269–277.

5. L. L. Yang, J. Zhou and L. S. Fu, *Dyes Pigments*, 2020, **174**, 108039.
6. J. F. Zhu, W. W. Yang, J. Yang and L. T. Jin, *J. Fluoresc.*, 2022, **32**, 397–404.
7. F. Leng, X. Zhang and J. H. Yu, *Dalton Trans.*, 2023, **52**, 5127–5140.
8. J. J. Liu, S. B. Xia, T. Liu, C. X. He, H. B. Suo and J. M. Liu, *J. Solid State Chem.*, 2021, **295**, 121900.
9. X. Y. Qiao, Y. F. Ge, Y. Y. Li, Y. Y. Niu and B. L. Wu, *ACS Omega*, 2019, **4**, 12402–12409.
10. A. H. Sun, Q. Wei, A. P. Fu, S. D. Han, J. H. Lia and G. M. Wang, *Dalton Trans.*, 2018, **47**, 6965–6972.
11. J. J. Liu, M. H. You, M. H. Li, C. C. Huang and M. J. Lin, *CrystEngComm*, 2020, **22**, 420–424.
12. S. D. Han, D. Wang, J. Pan, Q. Wei, J. H. Li and G. M. Wang, *Inorg. Chem.*, 2018, **57**, 11318–11321.
13. W. Zheng, Y. M. Tian, J. H. Zhang, S. X. Zhao and D. X. Jia, *Inorg. Chim. Acta*, 2021, **526**, 120542.
14. C. Y. Tang, W. Zheng, W. Q. Jiang and D. X. Jia, *Inorg. Chem. Commun.*, 2019, **104**, 23–26.
15. X. Y. Li, Y. L. Wang, Z. Xue, S. D. Han, Z. Z. Xue and J. Pan, *Cryst. Growth Des.*, 2021, **21**, 5261–5267.
16. C. Y. Yue, X. W. Lei, X. X. Lu, Y. Li, J. C. Wei, W. Wang, Y. D. Yin and N. Wang, *Dalton Trans.*, 2017, **46**, 9235–9244.
17. Z. Garda, E. Molnár, N. Hamon, J. L. Barriada, D. E. Gómez, B. Váradi, V. Nagy, K. Pota, F. K. Kálmán, I. Tóth, N. Lihi, C. P. Iglesias, É. Tóth, Tripier and G. Tircsó, *Inorg. Chem.*, 2021, **60**, 1133–1148.
18. S. Carli, E. Benazzi, L. Casarin, T. Bernardi, V. Bertolasi, R. Argazzi, S. Caramoria and C. A. Bignozzi, *Phys. Chem. Chem. Phys.*, 2016, **18**, 5949–5956.
19. R. Freitag and J. Conradie, *Electrochim. Acta*, 2015, **158**, 418–426.
20. M. B. Pineda, M. T. R. Silva, M. A. R. Romo, E. G. Vergara and A. R. Hernández, *Spectrochim. Acta Part A*, 2004, **60**, 1105–1113.
21. J. Conradie and K. G. Eschwege, *Data in Brief*, 2020, **31**, 105754.